Article

High genetic barrier to SARS-CoV-2 polyclonal neutralizing antibody escape

https://doi.org/10.1038/s41586-021-04005-0

Received: 1 July 2021

Accepted: 7 September 2021

Published online: 20 September 2021

Check for updates

Fabian Schmidt[1,4], Yiska Weisblum[1,4], Magdalena Rutkowska[2], Daniel Poston[1], Justin DaSilva[1], Fengwen Zhang[1], Eva Bednarski[1], Alice Cho[3], Dennis J. Schaefer-Babajew[3], Christian Gaebler[3], Marina Caskey[3], Michel C. Nussenzweig[2,3], Theodora Hatziioannou[1]✉ & Paul D. Bieniasz[1,2]✉

The number and variability of the neutralizing epitopes targeted by polyclonal antibodies in individuals who are SARS-CoV-2 convalescent and vaccinated are key determinants of neutralization breadth and the genetic barrier to viral escape[1–4]. Using HIV-1 pseudotypes and plasma selection experiments with vesicular stomatitis virus/SARS-CoV-2 chimaeras[5], here we show that multiple neutralizing epitopes, within and outside the receptor-binding domain, are variably targeted by human polyclonal antibodies. Antibody targets coincide with spike sequences that are enriched for diversity in natural SARS-CoV-2 populations. By combining plasma-selected spike substitutions, we generated synthetic 'polymutant' spike protein pseudotypes that resisted polyclonal antibody neutralization to a similar degree as circulating variants of concern. By aggregating variant of concern-associated and antibody-selected spike substitutions into a single polymutant spike protein, we show that 20 naturally occurring mutations in the SARS-CoV-2 spike protein are sufficient to generate pseudotypes with near-complete resistance to the polyclonal neutralizing antibodies generated by individuals who are convalescent or recipients who received an mRNA vaccine. However, plasma from individuals who had been infected and subsequently received mRNA vaccination neutralized pseudotypes bearing this highly resistant SARS-CoV-2 polymutant spike, or diverse sarbecovirus spike proteins. Thus, optimally elicited human polyclonal antibodies against SARS-CoV-2 should be resilient to substantial future SARS-CoV-2 variation and may confer protection against potential future sarbecovirus pandemics.

Neutralizing antibodies elicited by previous infection or by vaccination probably represent a key component of protective immunity against SARS-CoV-2. Antibodies targeting the receptor-binding domain (RBD) of the spike protein are thought to dominate the neutralizing activity of convalescent or vaccine recipient plasma[6], and include the most potent neutralizing antibodies cloned from individuals who are convalescent[7–11]. Nevertheless, additional SARS-CoV-2 neutralizing antibody targets include the N-terminal domain (NTD) and the fusion machinery[4,8,10,12,13], and the full spectrum of epitopes targeted by neutralizing antibodies in convalescent or vaccine recipient plasma has not been defined. SARS-CoV-2 variants of concern (VOCs) or variants of interest (VOIs) encode spike amino acid substitutions[14–17], some of which confer resistance to individual human monoclonal antibodies but have variable, typically modest, effects on neutralization by polyclonal plasma antibodies[1,6,9,17–20]. Mutated sites in VOCs include those in the RBD, NTD and elsewhere, but the numbers and locations of spike substitutions required for SARS-CoV-2 to evade the polyclonal neutralizing antibodies encountered in recipients of a vaccine or who are convalescent are unknown and are crucial determinants of population immunity.

Polyclonal neutralizing antibody targets

Exploiting the fact that SARS-CoV is poorly neutralized by SARS-CoV-2 convalescent plasma, we compared the sensitivity of HIV-1 pseudotypes bearing parental and chimeric spike proteins in which RBD sequences were exchanged (SARS-CoV-2(1-RBD) and SARS-CoV(2-RBD); Fig. 1a, Extended Data Fig. 1) to neutralization by plasma from 26 individuals from a previously described Rockefeller University COVID-19 convalescent cohort[21]. The plasma samples were obtained at an average of 1.3 months after infection and were selected for high SARS-CoV-2 neutralization titres (the RU27 plasma panel). Compared with the SARS-CoV-2 pseudotype, the SARS-CoV-2(1-RBD) pseudotype was less sensitive to neutralization by 21 of the 26 plasmas (median difference = 1.8-fold, range 0.5–9.8-fold, $P = 0.0005$ (Wilcoxon two-tailed test); Fig. 1b). Conversely, the SARS-CoV(2-RBD) pseudotype was more sensitive than the SARS-CoV pseudotype to all plasmas (median difference = 8-fold, range 1.2–75.5-fold, $P < 0.0001$ (Wilcoxon two-tailed test); Fig 1c). Nevertheless, the neutralizing potency of some plasmas was hardly affected when the SARS-CoV-2 RBD was replaced by the

[1]Laboratory of Retrovirology, The Rockefeller University, New York, NY, USA. [2]Howard Hughes Medical Institute, The Rockefeller University, New York, NY, USA. [3]Laboratory of Molecular Immunology, The Rockefeller University, New York, NY, USA. [4]These authors contributed equally: Fabian Schmidt, Yiska Weisblum. ✉e-mail: thatziio@rockefeller.edu; pbieniasz@rockefeller.edu

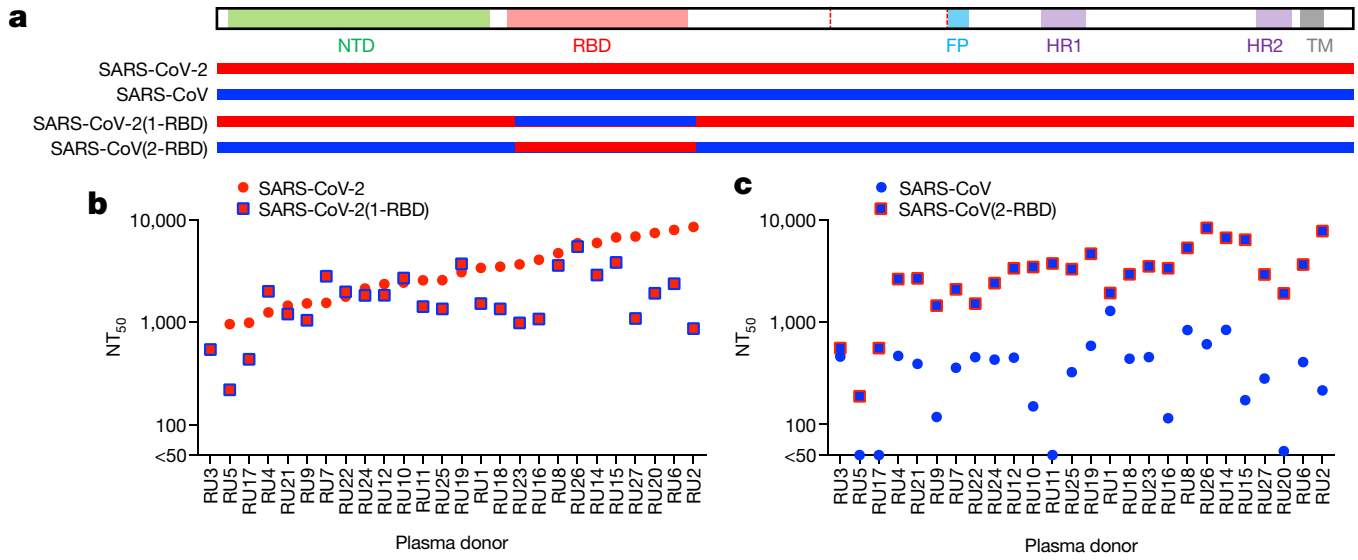

Fig. 1 | Neutralizing antibodies in SARS-CoV-2 convalescent plasma targeting both RBD and non-RBD determinants. a, Design of RBD-exchanged chimeric spike proteins. **b**, **c**, NT_{50} for 26 high-titre convalescent plasmas (from the RU1–27 panel) against pseudotyped HIV-1 virions bearing the indicated spike proteins. A median of two independent experiments is plotted. FP, fusion peptide; HR, heptad repeat; TM, transmembrane.

SARS-CoV RBD, even though some of those plasmas were minimally active against SARS-CoV (for example, RU9, RU10, RU11 and RU15; Fig. 1b, c). Indeed, plasmas that poorly neutralized SARS-CoV potently neutralized chimeric spike pseudotypes with either RBD or the other spike domains from SARS-CoV-2 (Fig. 1b, c). For the plasma panel as a whole, pseudotype neutralizing potency against SARS-CoV-2 did not correlate with potency against SARS-CoV or SARS-CoV-2(1-RBD), but did correlate with potency against SARS-CoV(2-RBD) (Extended Data Fig. 2a–c). Although altered conformation of the RBD in chimeric spike proteins might affect neutralization, these data indicate that while the RBD constitutes a major neutralizing target, substantial plasma neutralizing activity is also directed against non-RBD epitopes.

Polyclonal antibody-selected variants

To more precisely map the targets of polyclonal neutralizing antibodies in individuals who are convalescent, we passaged a recombinant vesicular stomatitis virus (rVSV)/SARS-CoV-2 chimeric virus[1,5] in the presence of each of the RU27 plasmas for up to six passages. rVSV/SARS-CoV-2 mimics the neutralization properties of SARS-CoV-2 (refs. [1,5]) but obviates the safety concerns that would accompany such studies with authentic SARS-CoV-2. Next-generation sequencing indicated that rVSV/SARS-CoV-2 passage in 22 out of the 27 plasmas led to the selection of spike mutants (Fig. 2a, Extended Data Fig. 3, Supplementary Table 1). For some plasmas, multiple substitutions were selected at distinct but proximal sites in viral subpopulations, indicating a dominant neutralizing activity targeting a particular epitope. For other plasmas, substitutions were enriched in multiple regions of the spike coding sequence, suggesting co-dominant neutralizing activities. Six passages of rVSV/SARS-CoV-2 without plasma enriched a small number of substitutions that were assumed to represent cell-culture or fitness-enhancing adaptations (for example, T604I), but were distinct from the majority of substitutions arising after rVSV/SARS-CoV-2 passage in plasma (Extended Data Fig. 3, Supplementary Table 1). Cumulatively, the plasma-selected mutations were enriched in specific elements within the NTD, RBD and other spike domains (Fig. 2a, Supplementary Table 1). From the 27 plasma-passaged virus populations, 38 individual mutant viruses were isolated by plaque purification; each encoded one, two or three spike substitutions (Fig. 2b) that generally occurred at high frequency in the passaged viral populations (Supplementary Table 1).

We compared the distribution of mutations selected by rVSV/SARS-CoV-2 passage with the RU27 plasma panel with those occurring in circulating SARS-CoV-2 populations (Fig. 2a–d). In both plasma-selected and naturally occurring sequences, substitutions were enriched in several elements that contribute to the 'supersite' targeted by NTD-binding neutralizing antibodies[12,13] (Fig. 2a–d). Similar plasma-selected and natural sequence variation was also evident in elements targeted by class 2 and class 3 RBD-binding neutralizing antibodies[22]. Mutations known to confer resistance to class I RBD antibodies were not selected by plasma passage, perhaps reflecting a lower than expected abundance of class I antibodies in this plasma panel (Fig. 2a–d). Other sites, including spike amino acids approximately 680–700 and approximately 930, exhibited variation in both plasma-passaged and natural variant datasets, but have not yet been demonstrated to be targeted by neutralizing antibodies. Nevertheless, the similarity in the distribution of natural and plasma-selected sequence variation within the spike protein suggests that selection by neutralizing antibodies is a driver of divergence in circulating SARS-CoV-2 populations.

Of the 38 plaque-purified rVSV/SARS-CoV-2 mutants recovered following passage in RU27 plasmas, 34 exhibited varying degrees of reduced sensitivity to neutralization by the plasma that was used for its selection (median 3.1-fold reduced half-maximal neutralizing titre (NT_{50}), range 0.8–39.3-fold; Extended Data Figs. 4, 5). Nevertheless, for 37 of the 38 selected rVSV/SARS-CoV-2 mutants, the selecting plasma exhibited residual neutralizing activity. We aggregated 13 mutations from the plasma-selected viruses based on their effects on plasma neutralization sensitivity (Extended Data Figs. 4, 5) and distribution throughout the spike protein, generating a single synthetic 'polymutant' spike (PMS) protein sequence, termed PMS1-1 (Extended Data Fig. 6a). An rVSV/SARS-CoV-2 derivative encoding these spike mutations (rVSV/SARS-CoV-2_{PMS1-1}) exhibited resistance to neutralization by the RU27 plasma panel that was greater in magnitude and consistency than the individual plasma-selected mutants (median 8.0-fold, range 2.7–52.9-fold; Fig. 2e). Nevertheless, 26 of the 27 RU27 plasmas retained residual neutralizing activity against rVSV/SARS-CoV-2_{PMS1-1} (Fig. 2e, Extended Data Fig. 6b). We conclude that some neutralizing epitopes are shared among the convalescent antibodies in high-titre plasmas,

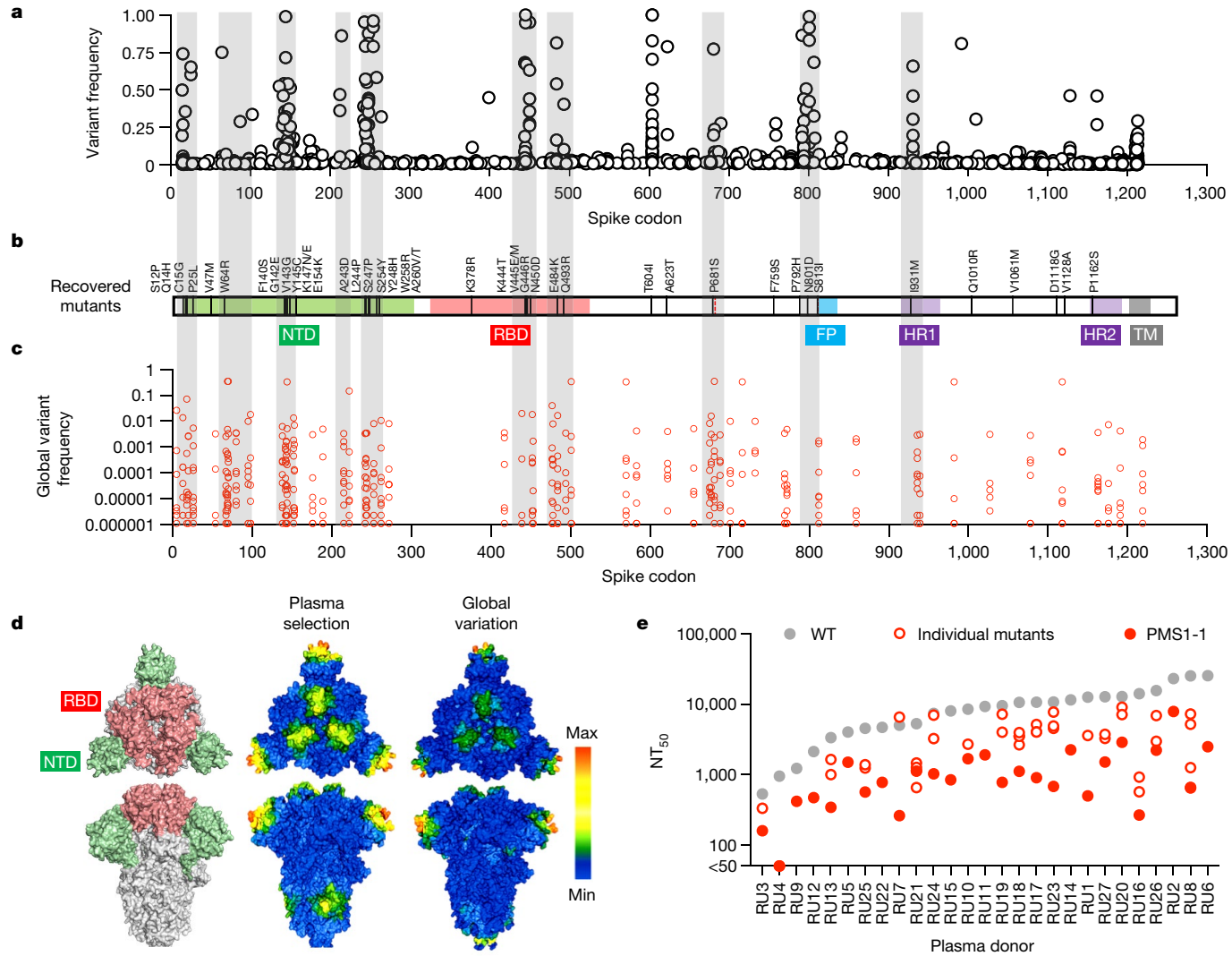

Fig. 2 | Selection of SARS-CoV-2 spike mutants by polyclonal antibodies. **a**, Frequencies of amino acid substitutions at each codon of the SARS-CoV-2 spike protein in two independent rVSV/SARS-CoV-2 populations (1D7 and 2E1), determined by Illumina sequencing. Pooled results following selection with the RU27 plasma panel are displayed. **b**, Locations of amino acid substitutions in 38 plaque-purified rVSV/SARS-CoV-2 isolates obtained from rVSV/SARS-CoV-2 populations following passage in the RU27 plasmas. **c**, Frequencies of naturally occurring amino acid substitutions (red circles) at each codon of the SARS-CoV-2 spike protein. The shaded grey bars in **a**–**c** indicate shared regions where variation is enriched. **d**, Comparison of the averaged frequency of substitutions observed after passaging rVSV/SARS-CoV-2 with RU27 plasmas (centre) and the frequency of sequence changes in natural populations (right), projected onto the SARS-CoV-2 spike structure (PDB 6VXX) with positions of the RBD and NTD indicated (left). The average frequency of substitutions in a 15 Å radius is represented using the colour spectrum (scale = 0–20 (centre) and 0–9 (right)). **e**, Neutralization potency of RU27 plasmas against rVSV/SARS-CoV-2 encoding wild type (WT), individually selected mutants or PMS1-1 spike proteins. A median of two independent determinations is plotted.

but neutralizing activity against SARS-CoV-2 is clearly polyclonal and heterogeneous among individuals with respect to epitope targets.

Polymutant and variant neutralization

We generated a panel of HIV-1 pseudotypes bearing the PMS1-1 spike protein, a second PMS protein with a different set of 13 mutations (selected based on similar criteria; known as PMSD4), or naturally occurring variants or relatives of the SARS-CoV-2 spike protein (Extended Data Fig. 7a, b). The panel included several SARS-CoV-2 VOC or VOI spike proteins, and spike proteins from sarbecoviruses found in bats (bCoV-RaTG13), pangolins (pCoV-GD and pCoV-GX) and previously in humans (SARS-CoV), that exhibit varying degrees of sequence divergence from SARS-CoV-2 (refs. [23–25]) (see Extended Data Fig. 1 for pseudotype characterization). To determine sensitivity and resistance to polyclonal SARS-CoV-2 antibodies, we used an independent set of 21 randomly selected (Ran1–21) convalescent plasmas, and a set of 14 plasmas from recipients who received an mRNA vaccine (Vac1–14), in addition to the RU27 high-titre plasma panel. The PMS spike proteins exhibited a degree of neutralization resistance that fell with the range of that exhibited by the four SARS-CoV-2 VOCs/VOIs and the four other sarbecoviruses (Extended Data Figs. 8a–c, 9a–c). Specifically, PMS1-1 and PMSD4 exhibited neutralization resistance that was greater than B.1.1.7 VOC and B.1.526 VOI, similar to P.1 VOC and less than B.1.351.3 VOC. PMS1-1 and PMSD4 were more resistant to neutralization than pCoV-GD and bCoV-RaTG13, both of which contain a larger number of changes relative to SARS-CoV-2 than the PMS spike proteins. Conversely, the pCoV-GX and SARS-CoV pseudotypes were more resistant to SARS-CoV-2 convalescent or vaccine recipient plasma than PMS1-1 and PMSD4 (Extended Data Figs. 8a–c, 9a–c). Notably, like PMS1-1 and PMSD4, the B.1.351.3 VOC that encodes only nine spike mutations relative to SARS-CoV-2 Wuhan-hu-1 was more resistant to neutralization than sarbecoviruses (pCoV-GD and bCoV-RaTG13) that contain a greater number of substitutions, suggesting that the B.1.351.3 mutations were selected by antibody pressure.

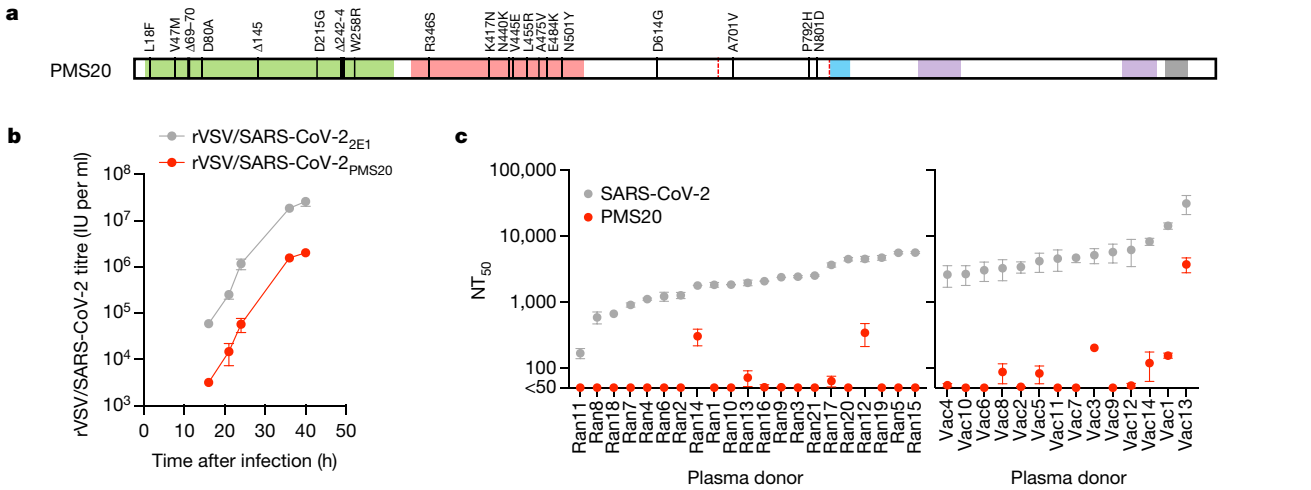

Fig. 3 | Neutralization resistance of polymutant SARS-CoV-2 spike proteins. **a**, Design of the PMS20 spike protein with 20 antibody-selected and VOC-associated mutations. **b**, Replication of rVSV/SARS-CoV-2 chimaeras encoding 2E1 (parental) or PMS20 spike proteins in 293T/ACE2cl.22 cells infected at a multiplicity of 0.001 and 0.008, respectively. **c**, Comparative neutralization potency of randomly selected convalescent (Ran1–21; left) and vaccine recipient (Vac1–14; right) plasmas, against Wuhan-hu-1 and PMS20 (**b**) SARS-CoV-2 HIV-1 pseudotypes. For **b** and **c**, the median ± range of two independent determinations is plotted.

A neutralization-resistant polymutant

On the basis of the above findings, we attempted to generate a mutant SARS-CoV-2 spike protein that was minimally divergent from SARS-CoV-2 Wuhan-hu-1, yet resistant to neutralization by polyclonal convalescent and vaccine recipient plasma. Successful derivation of such a spike protein would identify a complete list of neutralization epitopes recognized by polyclonal antibodies. We chose 20 naturally occurring mutations, including 8 NTD and 8 RBD changes (Fig. 3a) that either (1) arose in our plasma selection experiments (Fig. 2b), (2) occur in VOCs with reduced neutralization sensitivity (Extended Data Figs. 7, 8), or (3) arose in our previous studies in which human monoclonal antibody resistance was selected[1,2,9]. Naturally occurring deletion mutations in the NTD (Extended Data Fig. 7b), as well as multiple substitutions conferring resistance to classes 1, 2 and 3 RBD-binding antibodies[1,2,9] were included. An rVSV/SARS-CoV-2 derivative encoding the resulting spike sequence, termed PMS20 (Fig. 3a), was replication competent but attenuated compared with rVSV/SARS-CoV-2$_{2E1}$, suggesting that the 20 mutations confer a fitness cost (Fig. 3b). Nevertheless, HIV-1 pseudotypes bearing PMS20 were similarly infectious to those bearing the parental spike protein (Extended Data Fig. 1) and were highly resistant to neutralization. Indeed, 17 of the 21 random convalescent and 8 of the 14 mRNA vaccine recipient plasmas produced undetectable neutralization of PMS20 pseudotypes (less than 1:50; Fig. 3c). Among the high-titre convalescent RU27 plasmas, 23 of 27 had residual neutralizing activity against PMS20 that was reduced by a median of 32-fold compared with the parental pseudotype (range 2.8–114-fold; Extended Data Fig. 9a). We conclude that the 20 mutations in the PMS20 spike protein are sufficient for evasion of the majority of the antibodies in the plasma of individuals who have been infected by or vaccinated against SARS-CoV-2.

Polyclonal neutralization breadth

In contrast to plasmas from individuals who had been infected or vaccinated, a panel of plasmas from 14 individuals, termed 'infected-then-vaccinated' (ITV), who had been both infected by SARS-CoV-2 and subsequently received mRNA vaccines[3] retained neutralizing activity against HIV-1 pseudotypes bearing the PMS20 spike (Fig. 4a, b). Indeed, the PMS20 mutations that reduced Ran21 and Vac14 plasma NT$_{50}$ values by a median of 50-fold (range 5.9–225-fold) and 81-fold (range 8.4–229-fold), respectively, caused a median NT$_{50}$ reduction of only 18.6-fold (range 3.9–100-fold) for the ITV plasma panel (Fig. 4a, b). Analysis of chimeric SARS-CoV-2/PMS20 spike proteins in which the respective RBDs were exchanged (PMS20(2-RBD) and SARS-CoV-2(PMS-RBD)) indicated that the relative resistance of the PMS20 spike protein to both Ran and ITV plasmas was conferred by multiple spike determinants and that the neutralization breadth in the ITV plasmas was due to antibodies directed at both RBD and non-RBD determinants (Fig. 4a). In addition to the previously reported potent neutralizing activity of ITV plasmas against the B.1.1.7, B.1.525, P.1 and B.1.351.3 VOCs[3], the ITV plasmas also potently neutralized B.1.617.2 (delta), as well as a recently described variant (A.VOI.V2)[26] that has 11 substitutions and 3 deletions in the spike protein, including an extensively mutated NTD, and is predicted to be resistant to both class 2 and class 3 RBD-binding neutralizing antibodies (Extended Data Fig. 10a).

Plasma from the individuals who are ITV also had substantial neutralizing activity against heterologous sarbecovirus HIV-1 pseudotypes, including those that were poorly neutralized by Ran21, Vac14 and RU27 plasma panels and whose RBD and/or NTD sequences are extensively divergent from SARS-CoV-2 (Fig. 4c, Extended Data Fig. 10a, b). The median NT$_{50}$ values for the ITV plasmas against sarbecovirus pseudotypes were 5,330 (range 2,369–7,222) for bCoV-RaTG13, 3,617 (range 1,780–6,968) for pCoV-GX, 2,605 (range 1,386–3,181) for bCoV-WIV16 and 1,208 (range 621–2,705) for SARS-CoV (Fig. 4c, Extended Data Fig. 10a). Notably, the neutralizing activity of the ITV plasmas against the divergent sarbecoviruses bCoV-WIV16 and SARS-CoV was similar to that found in the random convalescent plasmas against SARS-CoV-2 Wuhan-hu-1. Thus, the neutralization potency and breadth of polyclonal plasma following mRNA vaccination of individuals who had previously been infected with SARS-CoV-2 seem greater than previously appreciated.

Discussion

These results indicate the presence of abundant neutralizing antibody targets on the SARS-CoV-2 spike protein. Our recent analyses further suggest that affinity maturation, over months of convalescence, confers antibody flexibility and affinity[2,3,27] and can impose a requirement for multiple viral substitutions for escape from individual neutralizing antibodies. Some human monoclonal antibodies thus have substantial activity against SARS-CoV-2 variants and divergent sarbecoviruses[2,28]. Overall, the diversity, maturity and high concentration of neutralizing antibodies probably explains why polyclonal plasma from individuals

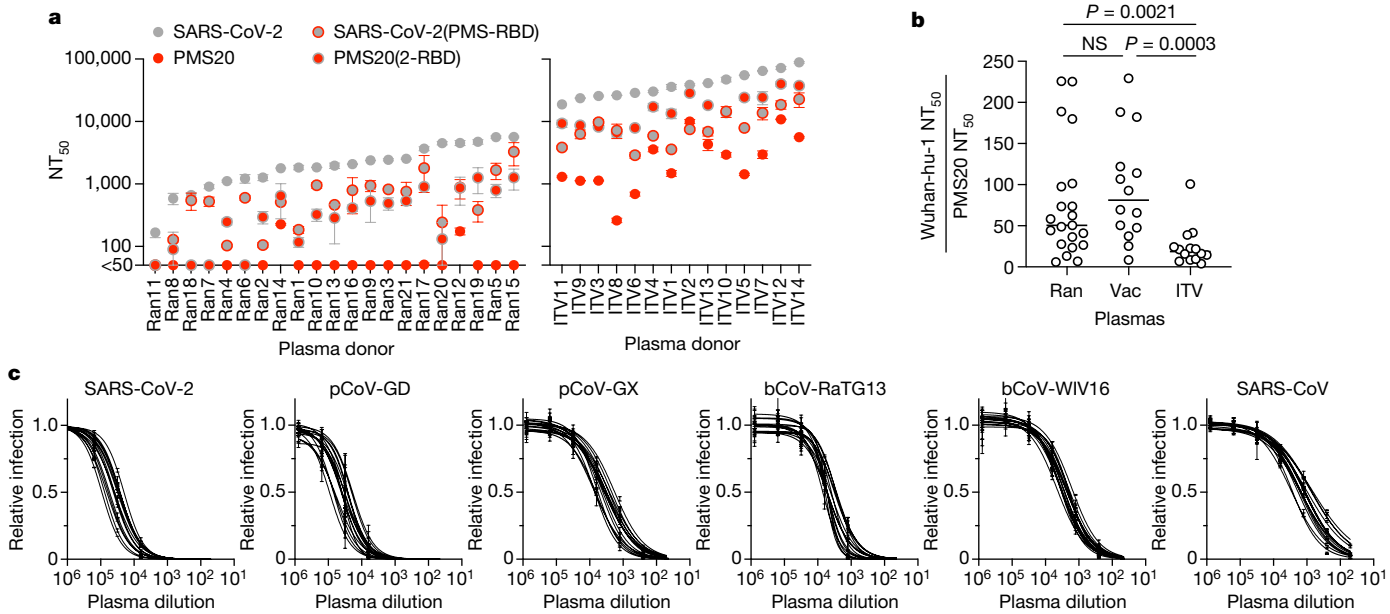

Fig. 4 | Neutralization breadth of polyclonal antibodies from ITV individuals. a, Comparative neutralization potency (NT_{50} values) of random convalescent (Ran1–21; left) and ITV (ITV1–14; right) plasmas against HIV-1 pseudotypes bearing SARS-CoV-2, PMS20 and RBD-exchanged chimeric spike proteins. **b**, Fold difference in NT_{50}, comparing neutralization of HIV-1 pseudotypes bearing SARS-CoV-2 and PMS20 spike proteins by Ran1–21, Vac1–15 and ITV1–14 plasmas (the *P* values were calculated using a two-sided Mann–Whitney test; horizontal lines indicate median values). **c**, Neutralization curves for ITV plasmas and the indicated sarbecovirus HIV-1 pseudotypes. For **a** and **c**, median ± range of two independent determinations is plotted.

who have been both infected and subsequently vaccinated could effectively neutralize the otherwise highly neutralization-resistant PMS20 polymutant, as well as sarbecoviruses that are divergent from SARS-CoV-2. While standard mRNA vaccine regimens may be less effective than infection at eliciting individual antibody breadth[29], it remains to be seen whether polyclonal neutralization potency and breadth can be achieved using appropriately timed boosting with existing SARS-CoV-2 vaccines. If so, existing immunogens may provide robust protection against future SARS-CoV-2 variants, and a degree of protection against diverse potential future sarbecovirus threats. Conversely, PMS proteins encoding numerous neutralization escape mutations may represent useful immunogens to broaden the polyclonal antibody response elicited by first-generation SARS-CoV-2 vaccines.

Online content

Any methods, additional references, Nature Research reporting summaries, source data, extended data, supplementary information, acknowledgements, peer review information; details of author contributions and competing interests; and statements of data and code availability are available at https://doi.org/10.1038/s41586-021-04005-0.

1. Weisblum, Y. et al. Escape from neutralizing antibodies by SARS-CoV-2 spike protein variants. *eLife* **9**, e61312 (2020).
2. Muecksch, F. et al. Affinity maturation of SARS-CoV-2 neutralizing antibodies confers potency, breadth, and resilience to viral escape mutations. *Immunity* **54**, 1853-1868.e7 (2021).
3. Wang, Z. et al. Naturally enhanced neutralizing breadth against SARS-CoV-2 1 year after infection. *Nature* **595**, 426–431 (2021).
4. Sauer, M. M. et al. Structural basis for broad coronavirus neutralization. *Nature Struct. Mol. Biol.* **28**, 478–486 (2021).
5. Schmidt, F. et al. Measuring SARS-CoV-2 neutralizing antibody activity using pseudotyped and chimeric viruses. *J. Exp. Med.* **217**, e20201181 (2020).
6. Greaney, A. J. et al. Comprehensive mapping of mutations in the SARS-CoV-2 receptor-binding domain that affect recognition by polyclonal human plasma antibodies. *Cell Host Microbe* **29**, 463–476 (2021).
7. Robbiani, D. F. et al. Convergent antibody responses to SARS-CoV-2 infection in convalescent individuals. *Nature* **584**, 437–442 (2020).
8. Rogers, T. F. et al. Isolation of potent SARS-CoV-2 neutralizing antibodies and protection from disease in a small animal model. *Science* **369**, 956–963 (2020).
9. Wang, Z. et al. mRNA vaccine-elicited antibodies to SARS-CoV-2 and circulating variants. *Nature* **592**, 616–622 (2021).
10. Liu, L. et al. Potent neutralizing antibodies against multiple epitopes on SARS-CoV-2 spike. *Nature* **584**, 450–456 (2020).
11. Cao, Y. et al. Potent neutralizing antibodies against SARS-CoV-2 identified by high-throughput single-cell sequencing of convalescent patients' B cells. *Cell* **182**, 1–12 (2020).
12. McCallum, M. et al. N-terminal domain antigenic mapping reveals a site of vulnerability for SARS-CoV-2. *Cell* **184**, 2332-2347.e16 (2021).
13. Cerutti, G. et al. Potent SARS-CoV-2 neutralizing antibodies directed against spike N-terminal domain target a single supersite. *Cell Host Microbe* **29**, 819-833.e7 (2021).
14. Fujino, T. et al. Novel SARS-CoV-2 variant identified in travelers from Brazil to Japan. *Emerg. Infect. Dis.* **27**, 1243–1245 (2021).
15. Volz, E. et al. Assessing transmissibility of SARS-CoV-2 lineage B.1.1.7 in England. *Nature* **593**, 266–269 (2021).
16. Tegally, H. et al. Detection of a SARS-CoV-2 variant of concern in South Africa. *Nature* **592**, 438–443 (2021).
17. West, A. P. et al. Detection and characterization of the SARS-CoV-2 lineage B.1.526 in New York. *Nat. Commun.* **12**, 4886 (2021).
18. Wibmer, C. K. et al. SARS-CoV-2 501Y.V2 escapes neutralization by South African COVID-19 donor plasma. *Nat. Med.* **27**, 622–625 (2021).
19. Tada, T. et al. Decreased neutralization of SARS-CoV-2 global variants by therapeutic anti-spike protein monoclonal antibodies. Preprint at *bioRxiv* https://doi.org/10.1101/2021.02.18.431897 (2021).
20. Andreano, E. et al. SARS-CoV-2 escape from a highly neutralizing COVID-19 convalescent plasma. *Proc. Natl Acad. Sci. USA* **118,** e2103154118 (2021).
21. Robbiani, D. F. et al. Recurrent potent human neutralizing antibodies to Zika virus in Brazil and Mexico. *Cell* **169**, 597-609.e11 (2017).
22. Barnes, C. O. et al. Structures of human antibodies bound to SARS-CoV-2 spike reveal common epitopes and recurrent features of antibodies. *Cell* **182**, 828-842.e16 (2020).
23. Zhou, P. et al. A pneumonia outbreak associated with a new coronavirus of probable bat origin. *Nature* **579**, 270–273 (2020).
24. Lam, T. T. et al. Identifying SARS-CoV-2-related coronaviruses in Malayan pangolins. *Nature* **583**, 282–285 (2020).
25. Zhang, T., Wu, Q. & Zhang, Z. Probable pangolin origin of SARS-CoV-2 associated with the COVID-19 outbreak. *Curr. Biol.* **30**, 1346-1351.e2 (2020).
26. de Oliveira, T. et al. A novel variant of interest of SARS-CoV-2 with multiple spike mutations detected through travel surveillance in Africa. Preprint at *medRxiv* https://doi.org/10.1101/2021.03.30.21254323 (2021).
27. Gaebler, C. et al. Evolution of antibody immunity to SARS-CoV-2. *Nature* **591**, 639–644 (2021).
28. Tortorici, M. A. et al. Broad sarbecovirus neutralization by a human monoclonal antibody. *Nature* **597**, 103–108 (2021).
29. Cho, A. et al. Anti-SARS-CoV-2 receptor binding domain antibody evolution after mRNA vaccination. *Nature* https://doi.org/10.1038/s41586-021-04060-7 (2021).

Methods

Cell lines

293T (American Type Culture Collection (ATCC) CRL-11268), 293T/ACE2cl.22 and HT1080/ACE2.cl.14 cells[5] were derived from original stocks purchased from the ATCC and were assumed to be authenticated by the ATCC. Cells were periodically checked for mycoplasma and retrovirus contamination by DAPI staining and reverse transcriptase assays, respectively.

SARS-CoV-2 and sarbecovirus spike protein pseudotyped reporter viruses

Plasmids pSARS-CoV-2-SΔ19 and pSARS-CoV-SΔ19 expressing C-terminally truncated SARS-CoV-2 (NC_045512) and SARS-CoV spike proteins have been previously described[5] and were used to construct the SARS-CoV-2(1-RBD) and SARS-CoV(2-RBD) expression plasmids in which RBD-encoding sequences were reciprocally exchanged. A panel of plasmids expressing spike proteins from SARS-CoV-2 VOC and VOI was constructed in the context of pSARS-CoV-2-SΔ19 (R683G)[5]. Substitutions were introduced using synthetic gene fragments (IDT) or overlap extension PCR-mediated mutagenesis and Gibson assembly. All VOCs/VOIs and polymutant spike proteins also included the R683G substitution, which disrupts the furin cleavage site and generates higher titre virus stocks without significant effects on pseudotyped virus neutralization sensitivity (Extended Data Fig. 1c, d). The potencies with which the plasma neutralized members of the mutant pseudotype panel were compared with potencies against a 'wild-type' SARS-CoV-2 spike sequence, carrying R683G where appropriate. Plasmids expressing the spike proteins found in the horseshoe bat (*Rinolophus affinis*) coronavirus bCoV-RaTG13 (ref. [23]) as well as the pangolin (*Manis javanica*) coronaviruses from Guangdong, China (pCoV-GD) and Guanxi, China (pCoV-GX)[24,25] were similarly constructed. Spike sequences were codon-modified to maximize homology with the human codon usage optimized of the pSARS-CoV-2 expressing plasmid VG40589-UT (Sinobiological). The 19-amino acid truncated coding sequence (CDS) of bCoV-RaTG13 (QHR63300), pCoV-GD (CoV_EPI_ISL_410721) and pCoV-GX (CoV_EPI_ISL_410542) were synthesized by GeneART and subcloned into pCR3.1 using NheI and XbaI and Gibson assembly, and referred to as pCR3.1-bCoV-RaTG13-SΔ19, pCR3.1pCoV-GD-SΔ19 and pCR3.1-pCoV-GX-SΔ19, respectively. Pseudotyped HIV-1 particles were generated as previously described[5]. Specifically, virus stocks were harvested 48 h after transfection of 293T cells with pHIV-1 GagPol and pCCNano/LucGFP (Fig.1) or pNL4-3ΔEnv-nanoluc (all other figures) along with a spike expression plasmid, filtered and stored at −80 °C.

SARS-CoV-2/sarbecovirus pseudotype neutralization assays

Plasmas were fivefold serially diluted and then incubated with pseudotyped HIV-1 reporter virus for 1 h at 37 °C. The antibody–pseudotype virus mixture was then added to HT1080/ACE2.cl14 cells. After 48 h, cells were washed with PBS, lysed with Luciferase Cell Culture Lysis reagent (Promega), and Nanoluc luciferase activity in lysates was measured using the Nano-Glo Luciferase Assay System (Promega) and a Glomax Navigator luminometer (Promega). The relative luminescence units were normalized to those derived from cells infected with the pseudotyped virus in the absence of plasma. The NT_{50} was determined using four-parameter non-linear regression (least squares regression method without weighting) (GraphPad Prism).

Plasma samples

Plasma samples were from individuals who were infected with SARS-CoV-2 for a mean of 1.3 months before plasma donation[7] or from individuals who had received mRNA vaccines at various times before plasma donation[9]. A set of 27 plasma samples from individuals infected with SARS-CoV-2 with high neutralizing activity who had not been vaccinated[7], termed the 'RU27' plasma panel, were used in VSV-SARS-CoV-2 selection procedures, while this panel plus a second set of 21 randomly selected plasmas (selected at random with blinding to neutralization titre or any demographic characteristic) from the same convalescent cohort formed the 'Ran21' plasma panel[7]. A set of 14 plasmas donated by individuals who had received a Pfizer/BioNTech mRNA vaccine formed the 'Vac14' plasma panel[9]. Finally, a set of 15 plasmas from individuals who were convalescent who had received a Pfizer/BioNTech mRNA vaccine between 6 and 12 months after infection[3] formed the infected-then-vaccinated 'ITV15' plasma panel. The study visits and blood draws were obtained with informed consent from all participants under a protocol that was reviewed and approved by the Institutional Review Board of the Rockefeller University (IRB no. DRO-1006, 'Peripheral Blood of Coronavirus Survivors to Identify Virus-Neutralizing Antibodies').

Selection of antibody-resistant rVSV/SARS-CoV-2 variants

To select plasma-resistant spike variants, rVSV/SARS-CoV-2/GFP_{1D7} and rVSV/SARS-CoV-2/GFP_{2E1} were passaged to generate diversity, and populations containing 10^6 plaque-forming units were incubated with plasma (diluted 1:50–1:400) for 1 h at 37 °C before inoculation of 2×10^5 293T/ACE2cl.22 cells in six-well plates. The following day, the medium was replaced with fresh medium containing the same concentrations of plasma. Supernatant from the wells containing the highest concentrations of plasma antibodies that showed evidence of rVSV/SARS-CoV-2/GFP replication (large numbers of GFP-positive cells or GFP-positive foci) was harvested 24 h later. Thereafter, aliquots (100 µl) of the cleared supernatant from the first passage (p1) were incubated with the same or increased concentration of plasma and then used to infect 2×10^5 293T/ACE2cl.22 cells in six-well plates, as before (p2). In situations where small but expanding GFP-positive foci were observed, the medium was refreshed at 48 h with fresh medium containing no plasma and the virus was harvested 24 h later. We repeated this process for up to six passages or until reduced neutralization potency for the plasma was obvious, as indicated by visual detection of increasing numbers of GFP-positive cells during passage.

To isolate individual mutant viruses by limiting dilution, the selected rVSV/SARS-CoV-2/GFP_{1D7} and rVSV/SARS-CoV-2/GFP_{2E1} populations were serially diluted in the absence of plasma and aliquots of each dilution added to individual wells of 96-well plates containing 1×10^4 293T/ACE2cl.22 cells. Individual viral variants were identified by observing single GFP-positive plaques in individual wells at limiting dilutions. The plaque-purified viruses were expanded, RNA was extracted and spike sequences were determined.

rVSV/SARS-CoV-2 neutralization assays

Plasma samples were fivefold serially diluted and then incubated with rVSV/SARS-CoV-2/GFP_{1D7} and rVSV/SARS-CoV-2/GFP_{2E1}, or plaque-purified selected variants thereof, for 1 h at 37 °C. The antibody–recombinant virus mixture was then added to 293T/ACE2.cl22 cells. After 16 h, cells were harvested, and infected cells were quantified by flow cytometry. The percentage of infected cells was normalized to that derived from cells infected with rVSV/SARS-CoV-2 in the absence of plasma. The NT_{50} for each plasma was determined using four-parameter non-linear regression (least squares regression method without weighting) (GraphPad Prism).

Sequence analyses

To identify putative antibody resistance mutations, RNA was isolated from aliquots of supernatant containing selected viral populations or individual plaque-purified variants using NucleoSpin 96 Virus Core Kit (Macherey-Nagel). The purified RNA was subjected to reverse transcription using random hexamer primers and the SuperScript VILO cDNA Synthesis Kit (Thermo Fisher Scientific). The cDNA was amplified using KOD Xtreme Hot Start DNA Polymerase (Millipore Sigma). Specifically, a fragment including the coding region of the extracellular domain of the spike protein was amplified using primers targeting the intergenic region between VSV-M and spike, and the spike intracellular domain. The PCR products were purified and sequenced either using Sanger sequencing or Illumina sequencing as previously described[30].

For Illumina sequencing, 1 µl of diluted DNA was used with 0.25 µl Nextera TDE1 Tagment DNA enzyme (15027865, Illumina) and 1.25 µl TD Tagment DNA buffer (15027866, Illumina). Then, the DNA was ligated to i5/i7 barcoded primers using the Illumina Nextera XT Index Kit v2 and KAPA HiFi HotStart ReadyMix (2X; KAPA Biosystems). Next, the DNA was purified using AmPure Beads XP (Agencourt), pooled and sequenced (paired end) using Illumina MiSeq Nano 300 V2 cycle kits (Illumina) at a concentration of 12 pM.

For analysis of the Illumina sequencing data, adapter sequences were removed from the raw reads and low-quality reads (Phred quality score of less than 20) using BBDuk. Filtered reads were mapped to the codon-optimized SARS-CoV-2 S sequence in rVSV/SARS-CoV-2/GFP and mutations were annotated using Geneious Prime (version 2020.1.2), using a *P* value cut-off of 10^{-6}. RBD-specific variant frequencies, *P* values and read depth were compiled using Python running pandas (1.0.5), numpy (1.18.5) and matplotlib (3.2.2). The parental rVSV/SARS-CoV-2/GFP 2E1 and 1D7 sequences each contain two adaptive mutations (F157S and R685M for 1D7; D215G and R683G for 2E1), but each was considered 'wild type' for the purposes of the plasma selection experiments and were subtracted from the analyses of the sequences.

The frequency of amino acid substitutions during rVSV/SARS-CoV-2 passage in plasmas was compared with the frequency of global occurrences of changes at each residue on 11 May 2021 (Los Alamos, COVID-19 Viral Genome Analysis Pipeline; https://cov.lanl.gov/content/index)[31]. For comparison of SARS-CoV-2 with sarbecoviruses, amino acid sequences were aligned with Clustal Omega. Using a python script clone of Simplot (https://jonathanrd.com/20-05-02-writing-a-simplot-clone-in-python/), the percent identity relative to SARS-CoV-2 was calculated within a rolling window of 100 amino acids, stepping a single residue at a time.

For three-dimensional sliding window analysis of changes in the spike amino acid sequence observed globally and in vitro, the frequency of global occurrences of changes at each residue (Los Alamos, COVID-19 Viral Genome Analysis Pipeline, https://cov.lanl.gov/content/index)[31] was divided by the average frequency of change at any reside and projected in the SARS-CoV-2 spike structure PDB 6VXX[32] as relative change frequency using BioStructMap[33,34]. Alternatively, the averaged frequency of substitutions observed after passaging rVSV/SARS-CoV-2 with plasma was divided by the mean substitution frequency and applied as a three-dimensional sliding window over the spike structure. The average frequency of substitutions in a 15 Å radius is represented using a colour spectrum.

Reporting summary

Further information on research design is available in the Nature Research Reporting Summary linked to this paper.

Data availability

Data on plasma-selected mutations are provided in Supplementary Table 1. Neutralization assay datasets generated during the current study are available in the accompanying supplementary source data files. Source data are provided with this paper.

Code availability

Analyses used commercially available software. No new code was generated

30. Gaebler, C. et al. Combination of quadruplex qPCR and next-generation sequencing for qualitative and quantitative analysis of the HIV-1 latent reservoir. *J. Exp. Med.* **216**, 2253–2264 (2019).
31. Korber, B. et al. Tracking changes in SARS-CoV-2 spike: evidence that D614G increases infectivity of the COVID-19 virus. *Cell* **182**, 812-827.e19 (2020).
32. Walls, A. C. et al. Structure, function, and antigenicity of the SARS-CoV-2 spike glycoprotein. *Cell* **181**, 281-292.e6 (2020).
33. Guy, A. J., Irani, V., Richards, J. S. & Ramsland, P. A. BioStructMap: a Python tool for integration of protein structure and sequence-based features. *Bioinformatics* **34**, 3942–3944 (2018).
34. Guy, A. J. et al. Proteome-wide mapping of immune features onto *Plasmodium* protein three-dimensional structures. *Sci. Rep.* **8**, 4355 (2018).

Acknowledgements This work was supported by US National Institutes of Health grants R37AI64003 and R01AI501111 (to P.D.B); R01AI78788 (to T.H.); and P01-AI138398-S1 and 2U19AI111825 (to M.C.N.). D.P. was supported by a Medical Scientist Training Program grant from the NIGMS (T32GM007739) to the Weill Cornell/Rockefeller/Sloan Kettering Tri-Institutional MD-PhD Program and by the NIAID (F30AI157898). C.G. was supported by the Robert S. Wennett Post-Doctoral Fellowship, in part by the National Center for Advancing Translational Sciences (National Institutes of Health Clinical and Translational Science Award programme, grant UL1 TR001866), and by the Shapiro–Silverberg Fund for the Advancement of Translational Research. P.D.B. and M.C.N. are Howard Hughes Medical Institute Investigators.

Author contributions P.D.B., T.H., M.C.N., F.S. and Y.W. conceived, designed and analysed the experiments. F.S. and Y.W. constructed and performed the rVSV/SARS-CoV-2 selection and neutralization experiments. F.S., Y.W., M.R., J.D.S. and E.B. performed the pseudotype neutralization experiments. F.S., T.H. and F.Z. constructed the expression plasmids. A.C. performed next-generation sequencing. D.P. and F.S. performed bioinformatic analysis. M.C., C.G. and D.J.S.-B. executed the clinical protocols, recruited participants and processed samples. P.D.B., T.H., F.S. and Y.W. wrote the manuscript with input from all co-authors.

Competing interests P.D.B. has received remuneration from Pfizer, Inc. for consulting on mRNA vaccines.

Additional information
Supplementary information The online version contains supplementary material available at https://doi.org/10.1038/s41586-021-04005-0.

Correspondence and requests for materials should be addressed to Theodora Hatziioannou or Paul D. Bieniasz.

Peer review information *Nature* thanks the anonymous reviewer(s) for their contribution to the peer review of this work.

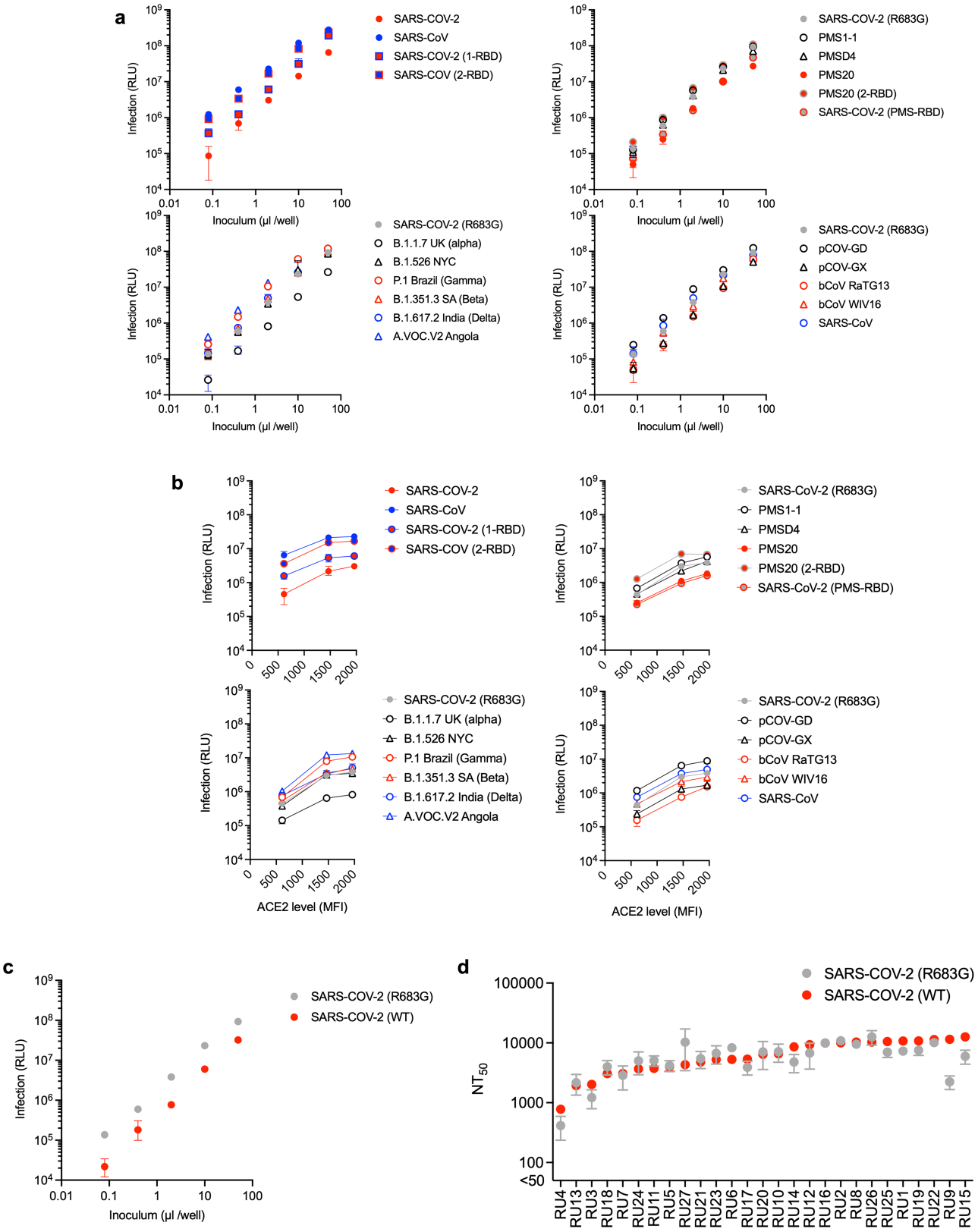

Extended Data Fig. 1 | See next page for caption.

Extended Data Fig. 1 | Characterization of HIV-1 pseudotypes bearing the chimeric, mutant, and variant SARS-CoV-2 and sarbecovirus spike proteins. a, Titration of pseudotyped viruses on 293T/ACE2cl.22 cells. Chimeric spike pseudotyped viruses in the upper left panel were built using the unaltered SARS-CoV-2Δ19 and SARS-CoVΔ19 spike protein constructs and a 3-plasmid HIV-1 pseudotyping system (see Methods). The other panels depict titration of pseudotypes derived using a furin cleavage site mutant SARS-CoV-2Δ19 spike protein (R683G) and a 2-plasmid HIV-1 pseudotyping system (see Methods). **b**, The same pseudotyped viruses used in (**a**) were used to infect 3 different 293T/ACE2 clonal cell lines each expressing a different level of ACE2 (MFI = mean fluorescence intensity). **c**, Titration of pseudotypes bearing an unaltered SARS-CoV-2Δ19 spike protein and a furin cleavage site mutant SARS-CoV-2Δ19 spike protein (R683G) generated using a 2-plasmid HIV-1 pseudotype system (see Methods). **d**, Comparative neutralization potency (NT_{50} values) of high titer convalescent (RU27) plasmas against HIV-1 pseudotypes bearing R683G mutant (grey symbols) and unaltered (red symbols) SARS-CoV-2Δ19 spike proteins. For all panels, median ± range of two independent experiments is plotted.

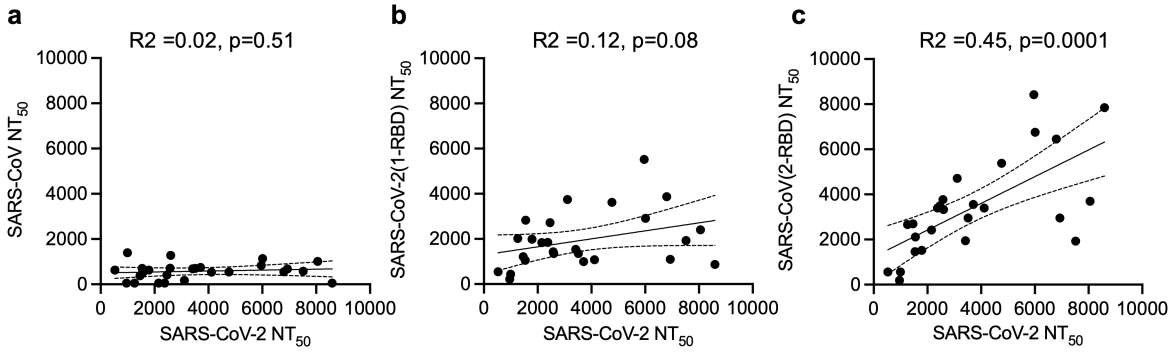

Extended Data Fig. 2 | The RU27 SARS-CoV-2 convalescent plasma panel contains neutralizing antibodies targeting RBD and non-RBD determinants. a–**c**, Correlations of neutralizing potencies of the RU27 plasmas against psudotypes bearing the indicated pairs of spike proteins. Simple linear regression was used to calculate R2 and p-values, dashed lines indicate 95% confidence intervals for the regression line.

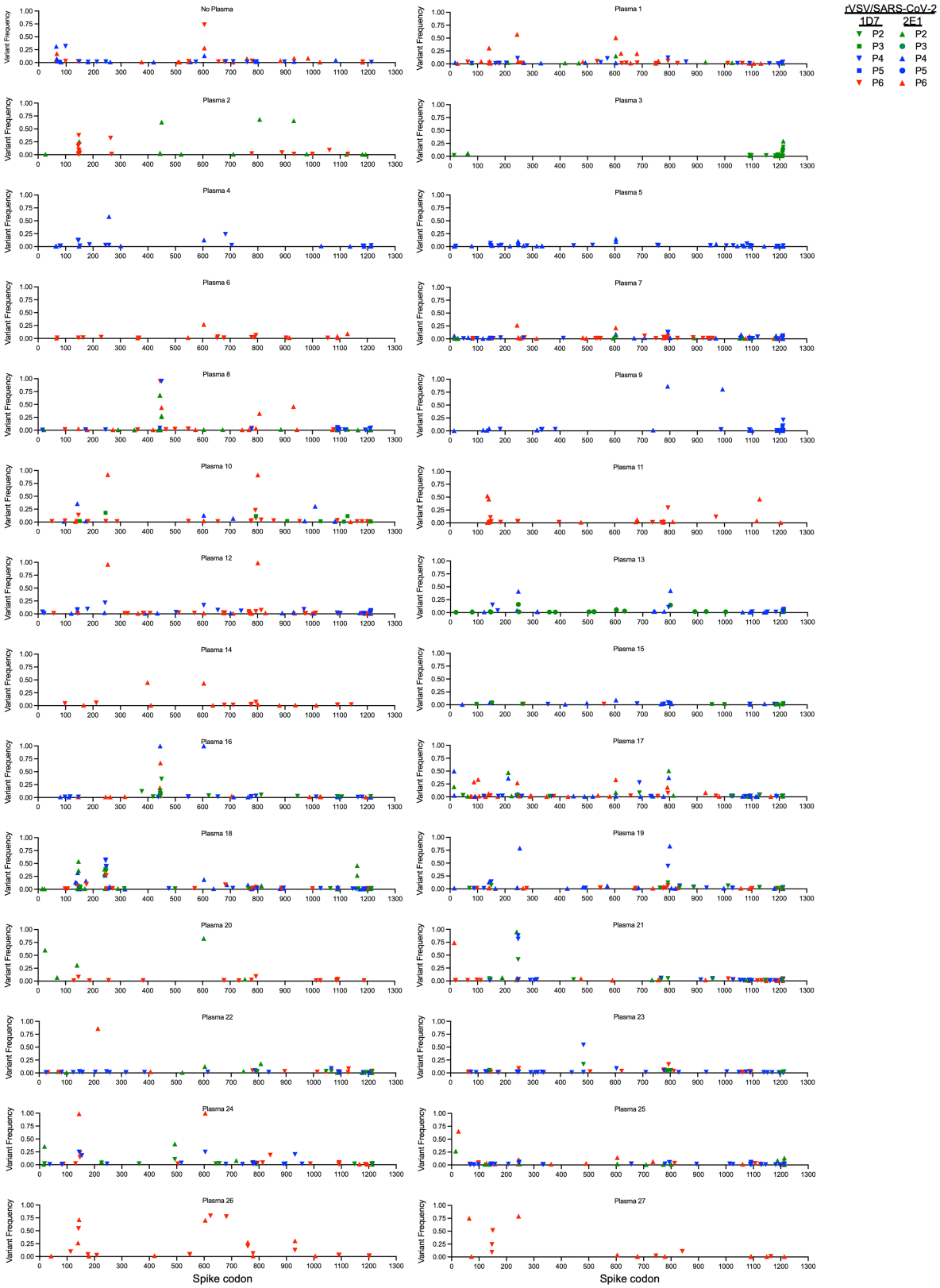

Extended Data Fig. 3 | Selection pressure on SARS-CoV-2 spike exerted by convalescent plasma. Frequencies of amino acid substitutions at each codon of the SARS-CoV-2 spike protein following the indicated number of passages (P2-P6) of two independent rVSV-SARS-CoV-2 populations (1D7 and 2E1), in each of the RU27 plasmas, determined by NGS sequencing.

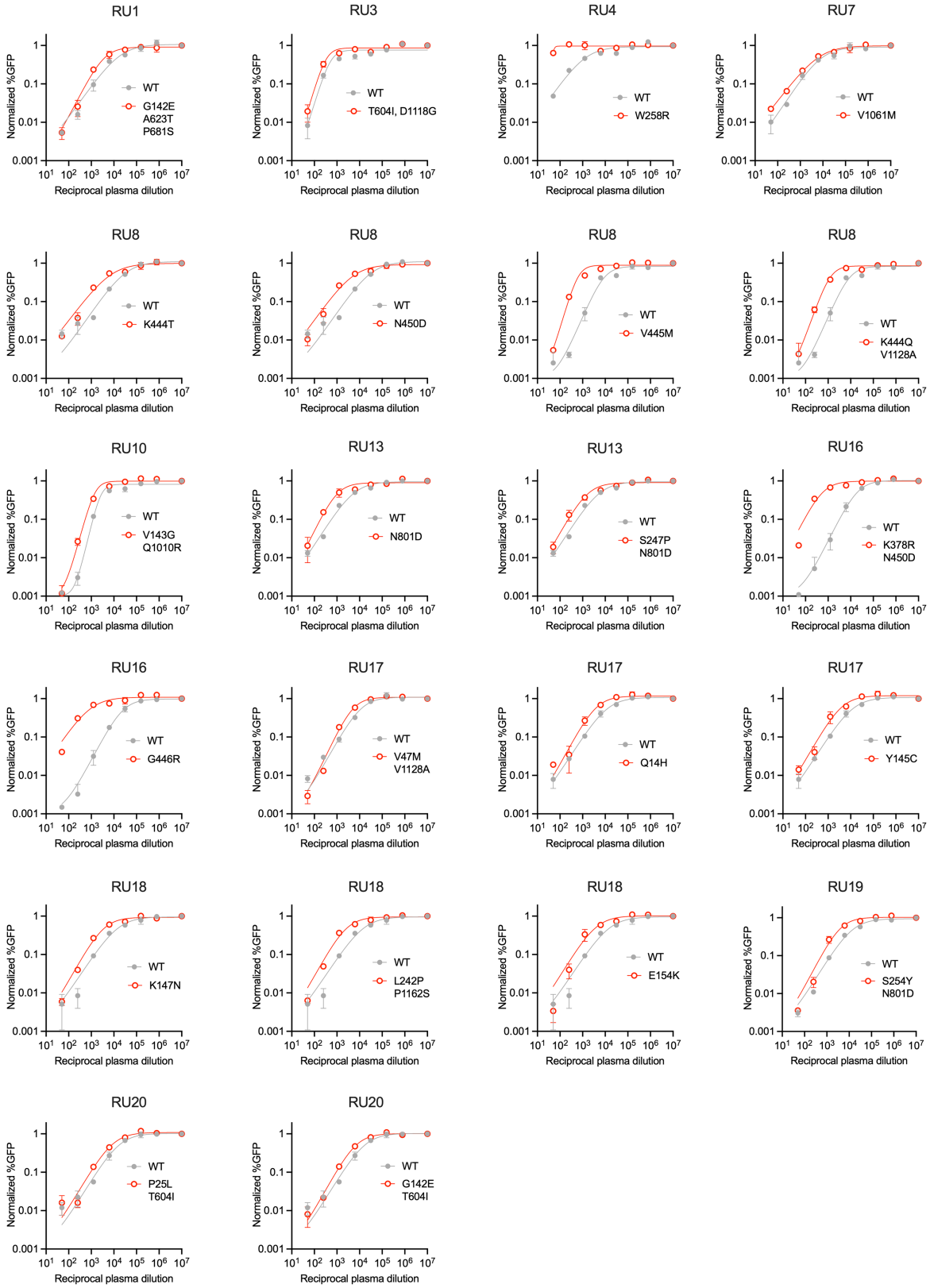

Extended Data Fig. 4 | Neutralization sensitivity of plasma-selected rVSV/SARS-CoV-2 mutants to RU1-20 plasmas. Infection, relative to non-neutralized controls, by plaque purified rVSV/SARS-CoV-2 isolates in the presence of the indicated dilutions of the indicated plasmas from the RU27 panel. The same plasmas that were used to select the indicated mutants were used to determine neutralization potency against the respective plaque purified mutants (red) and parental (WT, grey) rVSV/SARS-CoV-2 1D7 or 2E1 viruses. Median ± range of two technical replicates is plotted.

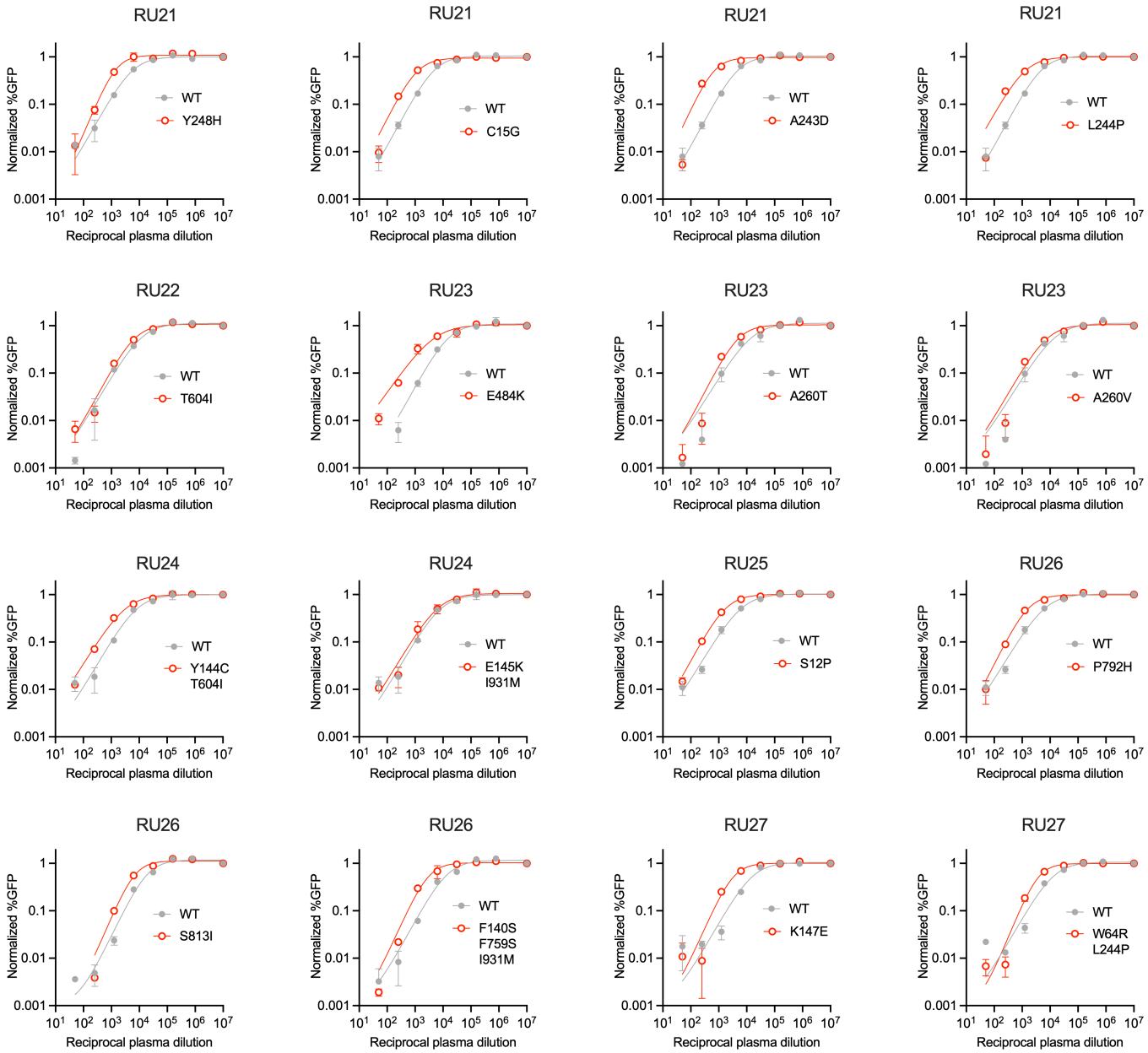

Extended Data Fig. 5 | Neutralization sensitivity of plasma-selected rVSV/SARS-CoV-2 mutants to RU 21-27 plasmas. Infection, relative to non-neutralized controls, by plaque purified rVSV/SARS-CoV-2 isolates in the presence of the indicated dilutions of the indicated plasmas from the RU27 panel. The same plasmas that were used to select the indicated mutants were used to determine neutralization potency against the respective plaque purified mutants (red) and parental (WT, grey) rVSV/SARS-CoV-2 1D7 or 2E1 viruses. Median ± range of two technical replicates is plotted.

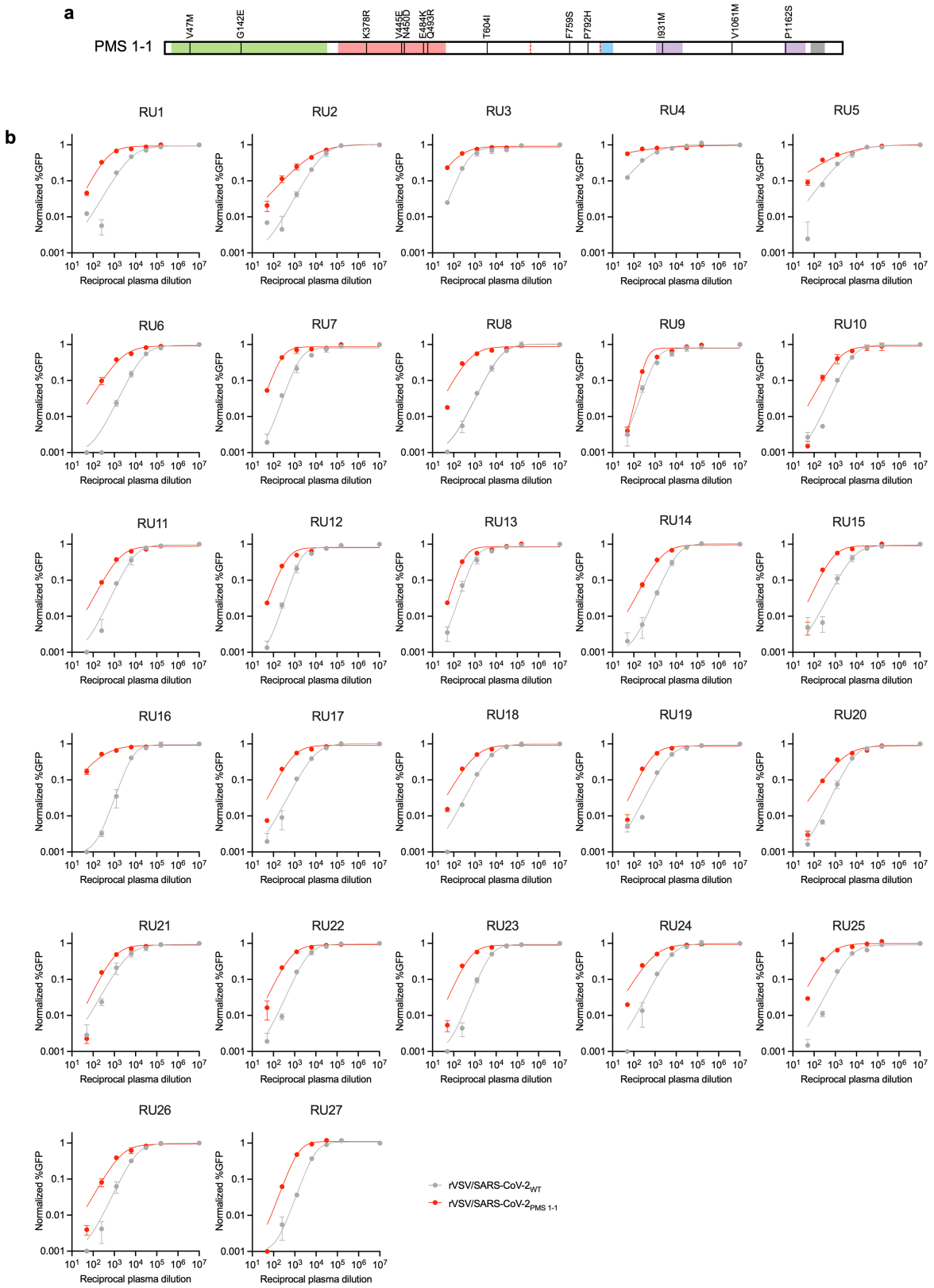

Extended Data Fig. 6 | Neutralization sensitivity of rVSV/SARS-CoV-2 encoding the PMS1-1 spike. a, Design of the PMS1-1 polymutant spike protein with 13 plasma-selected spike mutations aggregated in a single spike. **b**, Infection, relative to non-neutralized controls, by rVSV/SARS-CoV2$_{PMS1-1}$ (red) and rVSV/SARS-CoV2$_{2E1}$ (grey) in the presence on the indicated dilutions of the plasmas from the RU27 panel. Median ± range of two technical replicates is plotted.

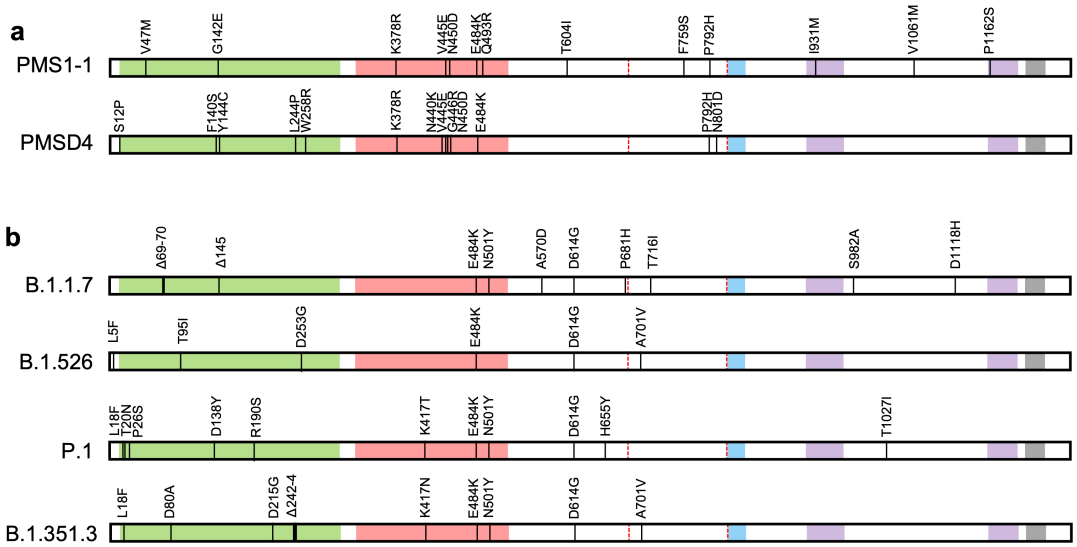

Extended Data Fig. 7 | Synthetic polymutant and natural variant SARS-CoV-2 spike proteins. a, Design of the PMS1-1 and PMSD4 polymutant spike proteins with 13 plasma-selected spike mutations aggregated in each spike. **b**, Schematic representation of mutations in naturally occurring VOC/VOI SARS-CoV-2 spike proteins.

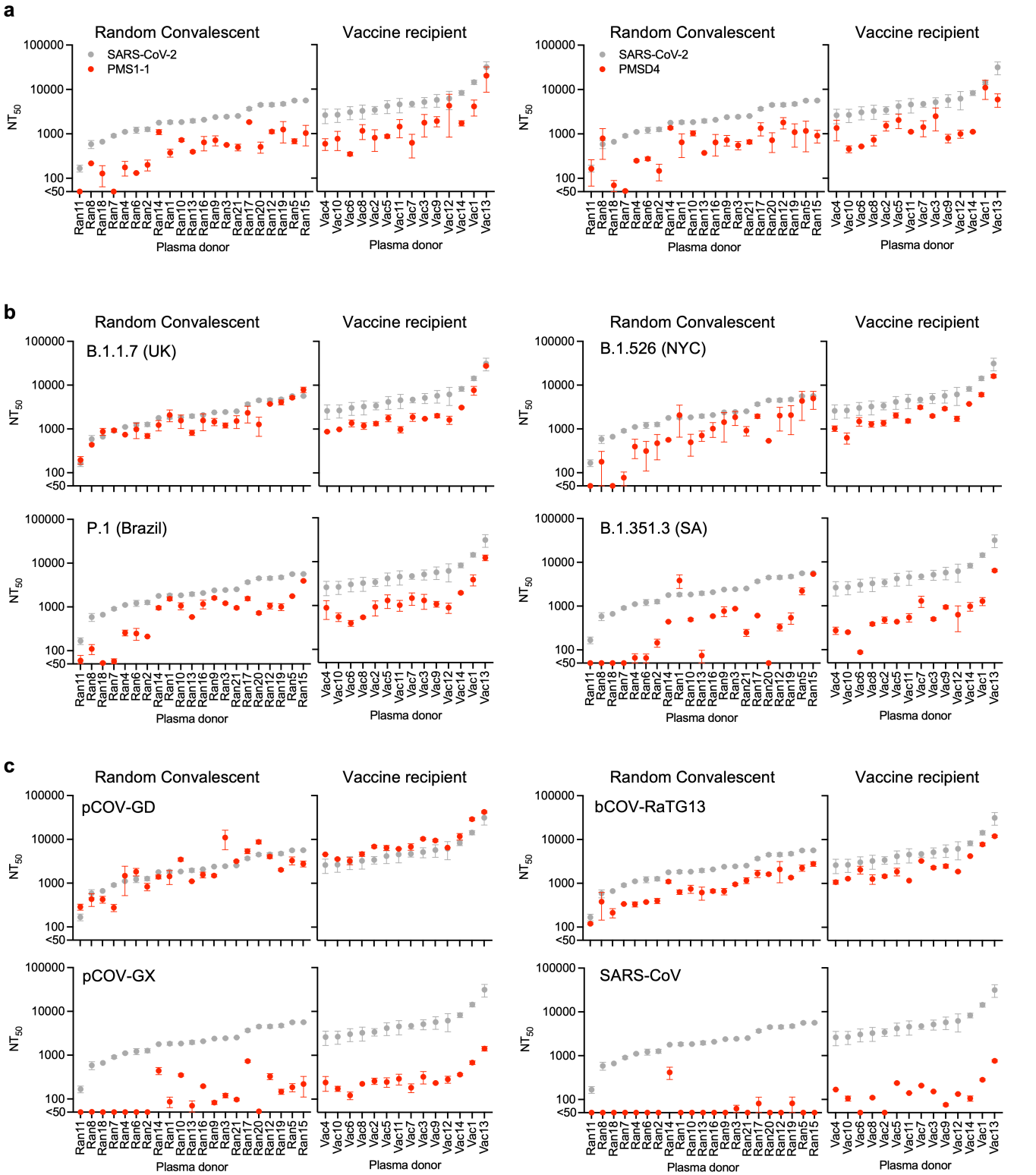

Extended Data Fig. 8 | Neutralization potency of random convalescent and vaccine recipient plasmas against polymutant, VOC/VOI, and sarbecovirus HIV-1 pseudotypes. a–**c**, Comparative neutralization potency (NT_{50} values) of random convalescent (Ran1-21) and vaccine recipient (Vac1-14) plasmas plasma against WT (grey symbols) and the indicated SARS-CoV-2 synthetic polymutant (**a**), natural variant (**b**) or sarbecovirus (**c**) (red symbol) HIV-1 pseudotypes. For all panels, median ± range of two independent experiments is plotted.

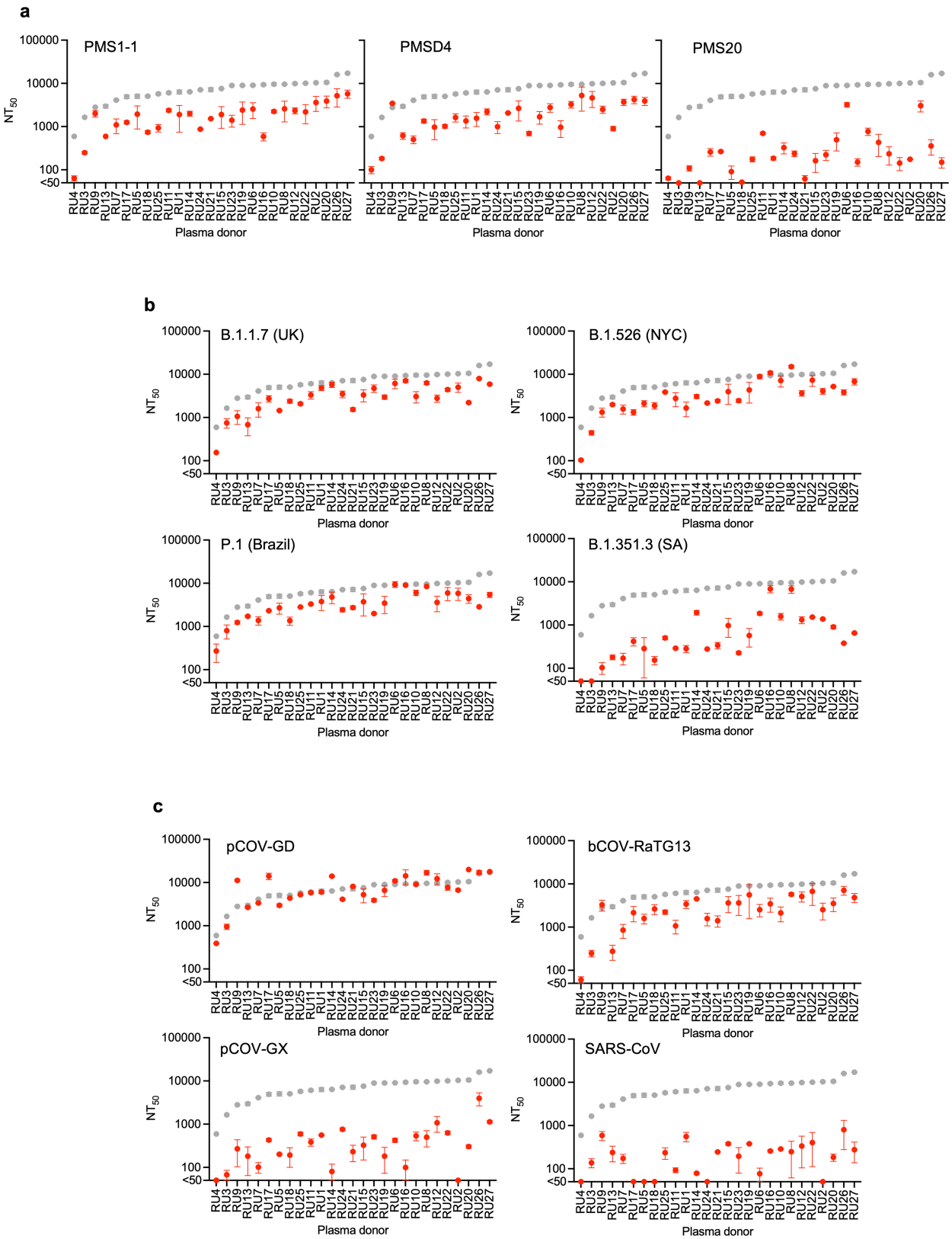

Extended Data Fig. 9 | Neutralization potency of high titer convalescent plasma against PMS, VOC/VOI, and sarbecovirus HIV-1 pseudotypes. **a**–**c**, Comparative neutralization potency (NT_{50} values) of high titer convalescent (RU27) plasma against WT (grey symbols) and indicated polymutant (**a**), SARS-CoV-2 natural variant (**b**) or sarbecovirus (**c**) (red symbol) HIV-1 pseudotypes. For all panels, median ± range of two independent experiments is plotted.

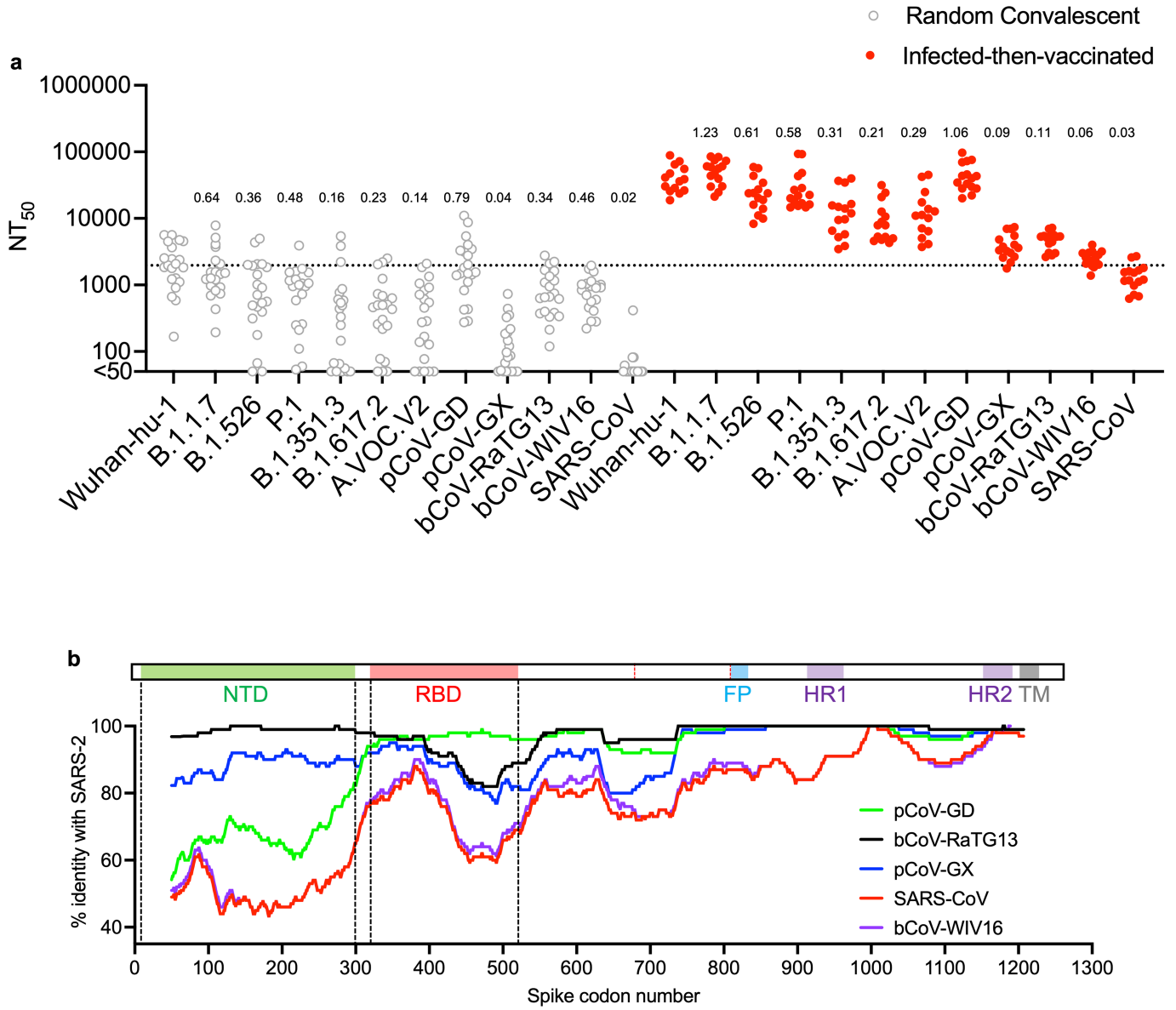

Extended Data Fig. 10 | Neutralization potency of plasma from infected-then-vaccinated against VOC/VOI and diverse sarbecovirus HIV-1 pseudotypes. a, Neutralization potency (NT_{50} values) of random convalescent plasmas (grey symbols) or ITV plasmas (red symbols) against SARS-CoV-2 prototype or variant or sarbecovirus HIV-1 pseudotypes. Median of two independent experiments is plotted. Dashed line indicated median NT_{50} for random convalescent plasmas against Wuhan-Hu-1 SARS-CoV-2. Numbers above each scatterplot indicate the median NT_{50} relative to the median NT_{50} for Wuhan-Hu-1 SARS-CoV-2. **b**, Sequence diversity across sarbecovirus spike domains; SARS-CoV-2 and the indicated sarbecovirus spike sequences were aligned with Clustal and compared using Simplot; the percent identity relative to SARS-CoV2 was plotted within a rolling window of 100 amino acids.

nature portfolio

Corresponding author(s): Hatziioannou and Bieniasz

Last updated by author(s): Sep 2, 2022

Reporting Summary

Nature Portfolio wishes to improve the reproducibility of the work that we publish. This form provides structure for consistency and transparency in reporting. For further information on Nature Portfolio policies, see our Editorial Policies and the Editorial Policy Checklist.

Statistics

For all statistical analyses, confirm that the following items are present in the figure legend, table legend, main text, or Methods section.

n/a	Confirmed	
☐	☒	The exact sample size (*n*) for each experimental group/condition, given as a discrete number and unit of measurement
☐	☒	A statement on whether measurements were taken from distinct samples or whether the same sample was measured repeatedly
☐	☒	The statistical test(s) used AND whether they are one- or two-sided *Only common tests should be described solely by name; describe more complex techniques in the Methods section.*
☒	☐	A description of all covariates tested
☒	☐	A description of any assumptions or corrections, such as tests of normality and adjustment for multiple comparisons
☒	☐	A full description of the statistical parameters including central tendency (e.g. means) or other basic estimates (e.g. regression coefficient) AND variation (e.g. standard deviation) or associated estimates of uncertainty (e.g. confidence intervals)
☒	☐	For null hypothesis testing, the test statistic (e.g. *F*, *t*, *r*) with confidence intervals, effect sizes, degrees of freedom and *P* value noted *Give P values as exact values whenever suitable.*
☒	☐	For Bayesian analysis, information on the choice of priors and Markov chain Monte Carlo settings
☒	☐	For hierarchical and complex designs, identification of the appropriate level for tests and full reporting of outcomes
☒	☐	Estimates of effect sizes (e.g. Cohen's *d*, Pearson's *r*), indicating how they were calculated

Our web collection on statistics for biologists contains articles on many of the points above.

Software and code

Policy information about availability of computer code

Data collection	Attune for FACS analysis of GFP expression. Glowmax Navigator Promega for naniluc assays
Data analysis	GraphPad Prism, BBDuk, Geneious Prime (Version 2020.1.2), Python running pandas (1.0.5), numpy (1.18.5), and matplotlib (3.2.2), python script clone of Simplot (https://jonathanrd.com/20-05-02-writing-a-simplot-clone-in-python/)

For manuscripts utilizing custom algorithms or software that are central to the research but not yet described in published literature, software must be made available to editors and reviewers. We strongly encourage code deposition in a community repository (e.g. GitHub). See the Nature Portfolio guidelines for submitting code & software for further information.

Data

Policy information about availability of data

All manuscripts must include a data availability statement. This statement should provide the following information, where applicable:

- Accession codes, unique identifiers, or web links for publicly available datasets
- A description of any restrictions on data availability
- For clinical datasets or third party data, please ensure that the statement adheres to our policy

The datasets generated during and/or analysed during the current study are available in supplementary table 1 or in the accompanying 'Source data' file

Field-specific reporting

Please select the one below that is the best fit for your research. If you are not sure, read the appropriate sections before making your selection.

☒ Life sciences ☐ Behavioural & social sciences ☐ Ecological, evolutionary & environmental sciences

For a reference copy of the document with all sections, see nature.com/documents/nr-reporting-summary-flat.pdf

Life sciences study design

All studies must disclose on these points even when the disclosure is negative.

Sample size	No sample size calculation was performed
Data exclusions	No data were excluded
Replication	All experiments were repeated independently at least twice, Each experiment was done with at least two technical replicates
Randomization	Not relevant
Blinding	No blinding was performed

Reporting for specific materials, systems and methods

We require information from authors about some types of materials, experimental systems and methods used in many studies. Here, indicate whether each material, system or method listed is relevant to your study. If you are not sure if a list item applies to your research, read the appropriate section before selecting a response.

Materials & experimental systems

n/a	Involved in the study
☒	☐ Antibodies
☐	☒ Eukaryotic cell lines
☒	☐ Palaeontology and archaeology
☒	☐ Animals and other organisms
☐	☒ Human research participants
☒	☐ Clinical data
☒	☐ Dual use research of concern

Methods

n/a	Involved in the study
☒	☐ ChIP-seq
☒	☐ Flow cytometry
☒	☐ MRI-based neuroimaging

Eukaryotic cell lines

Policy information about cell lines

Cell line source(s)	293T (ATCC CRL-11268) 293T/ACE2cl.22 Exp Med (2020) 217 (11): e20201181. https://doi.org/10.1084/jem.20201181 HT1080/ACE2.cl.14 J Exp Med (2020) 217 (11): e20201181. https://doi.org/10.1084/jem.20201181
Authentication	Not Authenticated after purchase from ATCC
Mycoplasma contamination	Negative for mycoplasma contamination (DAPI staining)
Commonly misidentified lines (See ICLAC register)	*Name any commonly misidentified cell lines used in the study and provide a rationale for their use.*

Human research participants

Policy information about studies involving human research participants

Population characteristics	As described previously Wang, Z., Schmidt, F., Weisblum, Y. et al. mRNA vaccine-elicited antibodies to SARS-CoV-2 and circulating variants. Nature 592, 616–622 (2021). https://doi.org/10.1038/s41586-021-03324-6
Recruitment	As described previously: Wang, Z., Schmidt, F., Weisblum, Y. et al. mRNA vaccine-elicited antibodies to SARS-CoV-2 and circulating variants. Nature 592, 616–622 (2021). https://doi.org/10.1038/s41586-021-03324-6
Ethics oversight	Institutional Review Board of the Rockefeller University; protocol DRO-1006

Note that full information on the approval of the study protocol must also be provided in the manuscript.